



ROBUST FUNCTIONAL BEAMFORMING

Robert P. Dougherty¹

¹OptiNav, Inc.

1414 127th PL NE #106, 98005, Bellevue, WA, USA

ABSTRACT

Functional Beamforming (FB) offers excellent dynamic range, giving very small results, instead of the usual sidelobes, when the computed steering vectors match the normalized Green's functions of the actual acoustic sources. It can be proven that FB result will not be less than the correct result if the steering vector is accurate. Unfortunately, small errors in the computed steering vector resulting from imperfect knowledge of or randomness in the acoustic propagation can cause the FB output to be significantly reduced from the correct value, especially if the FB exponent, ν , is large. In practice, this constrains ν and consequently the dynamic range benefit of the method. This paper presents a way to adjust the steering vector to increase the BF output. A The method of steepest ascent is applied, moving the steering vector to increase the output. The length of the step is either the distance to the first maximum of the FB expression or a specified limit, ϵ , whichever is smaller. The resulting method, Robust Functional Beamforming, RBF, has been shown in testing to offer both high dynamic range and low output loss if the two parameters, ν and ϵ are chosen correctly.

1 METHOD AND DERIVATION

Let the array cross spectral matrix be denoted \mathbf{C} and the normalized steering vector in the beamforming grid be \mathbf{g} . The Functional Beamforming (FB) expression [1-4] for estimating the strength of the source associated with \mathbf{g} is

$$b_\nu(\mathbf{g}) = \left[\mathbf{g}' \mathbf{C}^{\frac{1}{\nu}} \mathbf{g} \right]^\nu \quad (1)$$

where $1 \leq \nu \leq \infty$. From the operator monotone nature of the function $f(t) = t^{\frac{1}{\nu}}$ on $0 \leq t < \infty$, it follows that if $\mathbf{C} \geq s \mathbf{g} \mathbf{g}'$, then $b_\nu(\mathbf{g}) \geq s$. However if $\mathbf{C} = s \mathbf{h} \mathbf{h}'$ where \mathbf{h} differs from \mathbf{g} such that $|\mathbf{g}' \mathbf{h}|^2 = \cos^2 \theta$, then $b_\nu(\mathbf{g}) = \cos^{2\nu} \theta s$. For example, suppose $\theta = 10^\circ$ and $\nu =$

80. Then $\cos^{2\nu}\theta = 0.0863 = -10.6$ dB. In this case the error in \mathbf{g} is $\mathbf{x} = \mathbf{h} - \mathbf{g}$. Assuming, without loss of generality that $\mathbf{g}'\mathbf{h}$ is real and positive, then $\|\mathbf{x}\| = \sqrt{2(1 - \cos\theta)}$. For an angle of 10° , $\|\mathbf{x}\| = 0.17$. Adjusting \mathbf{g} by moving this distance in a direction parallel to $\mathbf{h} - \mathbf{g}$ could produce a 10.6 dB increase in the beamformer output.

Steering vector errors have several common sources. One is a beamforming grid that is too coarse, so that the peak is missed in between the grid points. Another frequent source of error relates to the microphone array design. For example, a grid-like structure holding the microphones gives rise to diffraction effects that alter the measured phase relative to the ideal Green's function. A finite, solid, planar array can do the same thing. The microphones can have intrinsic phase differences between them. In a wind tunnel, nonuniform flow can alter the propagation paths on a steady or unsteady basis. Non-simple sources can have directivity functions that differ from a monopole model significantly over the extent of the array.

Compensating for imperfect steering vectors is standard practice in adaptive beamforming, which is even more sensitive to errors than FB is. The approach of loading the diagonal by Tikhonov regularization leads to Robust Adaptive Beamforming [5]. Experience has shown that this is not very helpful for FB. An explanation is that effect of diagonal loading is to round off the peak of the point spread function, but FB does not need this treatment because the peak is already round. A method called Robust Capon beamforming corrects the steering vectors by changing them slightly to increase the beamforming output [5]. The amount of movement is constrained to an ellipsoidal set, and the method of Lagrange multipliers is applied to the resulting optimization problem.

In the presentation here, the method of steepest ascent is used to move the steering vector in a straight line in array space until either a local maximum is attained or a limit on the amount of steering vector change, a trust radius, has been reached. This is done inside the $[\]^\nu$ bracket of FB, so there is strong effect of increasing the function.

In order to change \mathbf{g} without handling a separate constraint on its length to keep it normalized, the function to be maximized is

$$b^{\frac{1}{\nu}}(\mathbf{g}) = \frac{\mathbf{g}'\mathbf{C}^{\frac{1}{\nu}}\mathbf{g}}{\mathbf{g}'\mathbf{g}} \quad (2)$$

where the $[\]^\nu$ operation is postponed and the \cdot . The steepest ascent direction is given by the gradient with respect to \mathbf{g}' so as to produce a complex column vector

$$\nabla_{\mathbf{g}'} b^{\frac{1}{\nu}} = \mathbf{C}^{\frac{1}{\nu}}\mathbf{g} - \left(\mathbf{g}'\mathbf{C}^{\frac{1}{\nu}}\mathbf{g}\right)\mathbf{g} \quad (3)$$

Normalizing the resulting direction vector gives

$$\mathbf{a} = \frac{\mathbf{g}'\mathbf{C}^{\frac{1}{\nu}}\mathbf{g} - \left(\mathbf{g}'\mathbf{C}^{\frac{1}{\nu}}\mathbf{g}\right)\mathbf{g}}{\sqrt{\mathbf{g}'\mathbf{C}^{\frac{2}{\nu}}\mathbf{g} - \left(\mathbf{g}'\mathbf{C}^{\frac{1}{\nu}}\mathbf{g}\right)^2}} \quad (4)$$

Conveniently, \mathbf{a} is orthogonal to \mathbf{g} . The value Eq. (2) along the line $\mathbf{x} = t\mathbf{a}$ is

$$b^{\frac{1}{v}}(\mathbf{g} + t\mathbf{a}) = \frac{\mathbf{g}'\mathbf{C}^{\frac{1}{v}}\mathbf{g} + \left(\mathbf{g}'\mathbf{C}^{\frac{1}{v}}\mathbf{a} + \mathbf{a}'\mathbf{C}^{\frac{1}{v}}\mathbf{g}\right)t + \mathbf{a}'\mathbf{C}^{\frac{1}{v}}\mathbf{a}t^2}{1 + t^2} \quad (5)$$

It is straightforward to find the values of t_{peak} for which Eq. (5) reaches its peak. To simplify the expression let

$$\alpha = \mathbf{a}'\mathbf{C}^{\frac{1}{v}}\mathbf{a}, \quad \gamma = \mathbf{g}'\mathbf{C}^{\frac{1}{v}}\mathbf{g}, \quad \kappa = \mathbf{g}'\mathbf{C}^{\frac{1}{v}}\mathbf{a} \quad (6)$$

Then

$$t_{peak} = \frac{\alpha - \gamma + \sqrt{(\alpha - \gamma)^2 + (\kappa + \kappa^*)^2}}{\kappa + \kappa^*} \quad (7)$$

The positive root of the quadratic equation is selected because this is the appropriate one. Given a maximum t -limit, ϵ the output of RFB, is obtained by evaluating Eq. (5) at t_{peak} or ϵ , whichever is smaller, and raising the result to the power v .

It is possible to apply Eq. (5) by using an algebraic expression for the updated beamforming result. However, in context of deconvolution, it is preferable to explicitly compute and normalize the new steering vectors $\mathbf{g} + t\mathbf{a}$ so that the various updated steering vectors in the grid can be used to update the point spread function. In this way, the deconvolution is still logically consistent, only based on the revised steering vectors instead of the original ones. This should compensate for the increased raw beamformer output in computing the final, quantitative, result.

The new method is called Robust Functional Beamforming (RFB). Examples of its use are given in references [8] and [9].

2 SAMPLE RESULTS

Real data, instead of simulations, is used to illustrate the performance of the method. The first uses a 40 element acoustic camera with a 30 cm aperture imaging the loudspeaker near the center of Fig. 1.

In this example, inaccurate steering vectors are created by using a beamforming grid that is deliberately made to be too coarse. The nominal grid size for processing this data has a grid spacing of 3.5 mm, but 20×20 binning is used to produce a grid size of 70 mm. The meaning of binning in this case is that a coarse grid was used for beamforming and the resulting values were used to fill in the unused points. Results for 3 kHz with $v=80$ and $\epsilon = 0$ and 0.02 are shown in Fig. 2.

The peak levels in the speaker ROI, the green box in Fig. 2, as a function of frequency are shown in Fig. 3, along with the median microphone spectrum. For a given frequency, the RFB output increases with ϵ up to a point and then stops increasing. The limiting value is slightly below the array median because the array data include other sources and propagation paths in addition to sources in the green ROI. The noise is broadband and the analysis bands are somewhat wide (1/12th OB), so reflection effects that would reduce the array median relative to the ROI sources are not expected in this case. The fan source in the picture was turned off.

The effect of ϵ on the point spread function is illustrated in Fig. 4 by showing horizontal profiles of unbinned RFB plots through the speaker for a single frequency, $\nu = 80$, and several values of ϵ . The peak aligns with the tweeter component of the speaker at $x = 1.723$ m. The PSF for $\epsilon = 0.02$ is almost a rectangular box, which may be the most desirable shape for a PSF intended for quantitative measurements.



Fig. 1 Loudspeaker test setup.

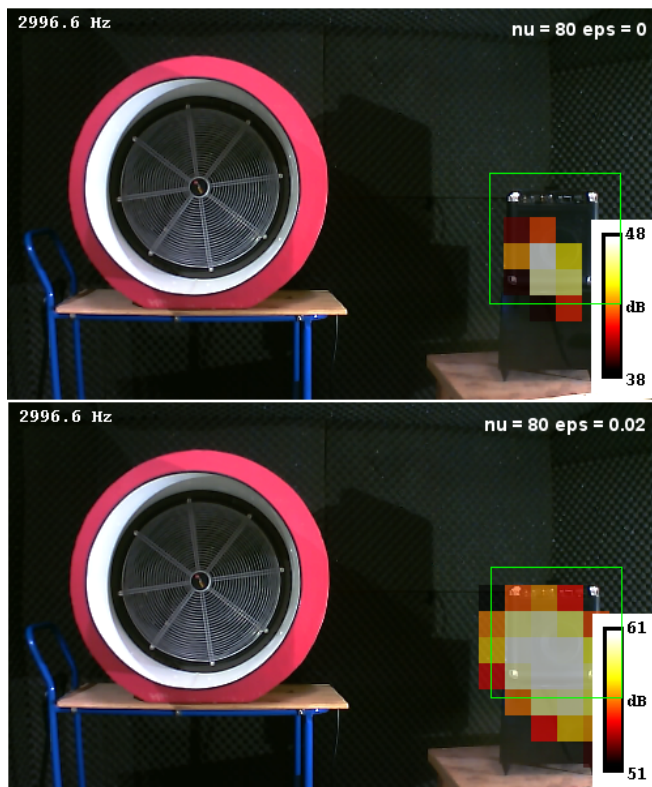


Fig. 2 Binned RFB for 3 kHz using $\nu = 80$ and $\epsilon = 0$ (top) and 0.02 (bottom).

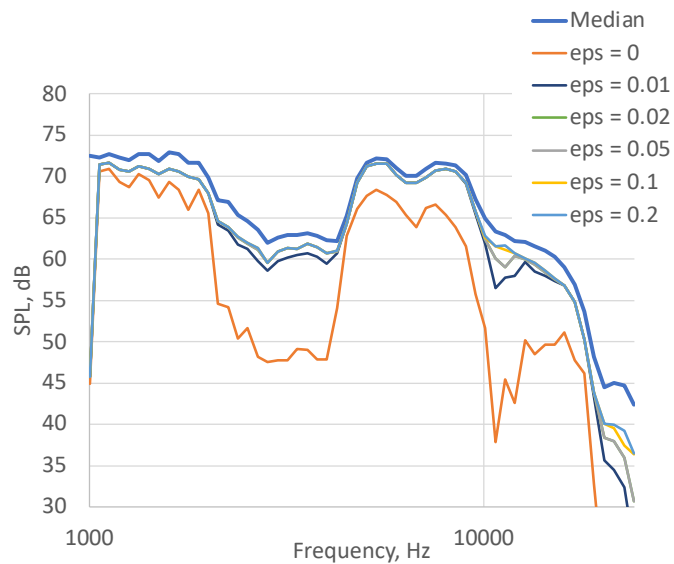


Fig. 3 Peak RFB levels for the speaker data with $\nu = 80$ and binned beamforming as functions of frequency and ϵ . The median spectrum for the array microphones is also shown.

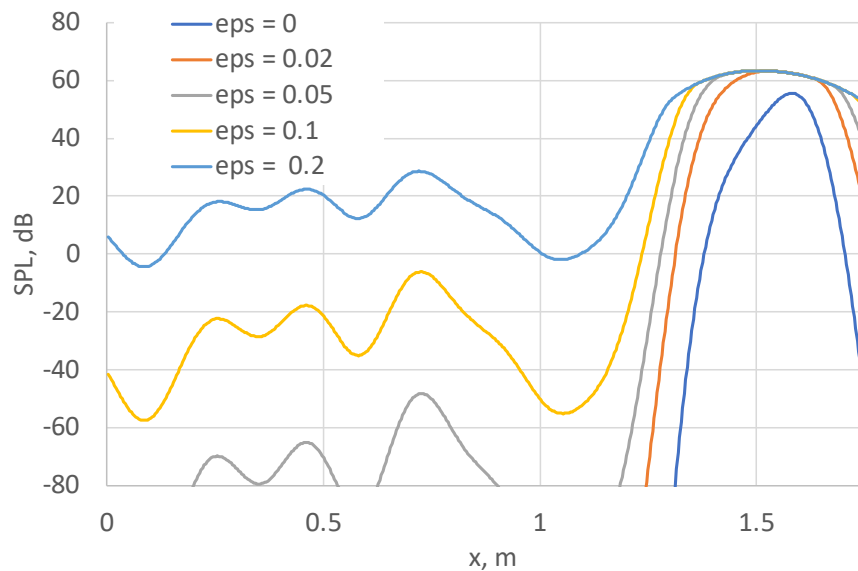


Fig. 4 Horizontal profiles of the RFB map for the speaker at 10 kHz. levels for the speaker data with $\nu = 80$ functions of frequency and ϵ . The tweeter element of the speaker is at $x = 1.723$ m.

Robust Functional Beamforming plots for the DLR 1 beamforming benchmark data [6&7] are given in Fig. 5. In these high frequency plots RFB has dynamic range with the preservation of levels of conventional beamforming.

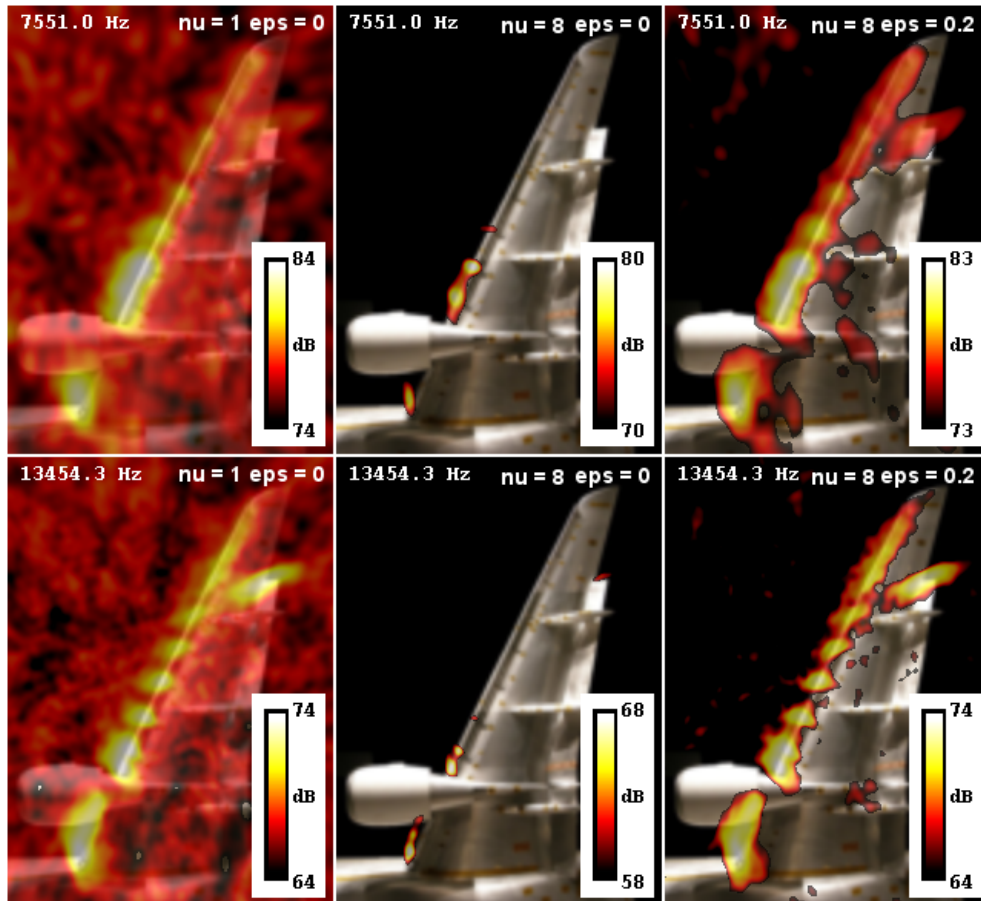


Fig. 5 Robust Functional Beamforming plots for DLR 1 benchmark data. The top row is for 7551 Hz and the bottom row is 13454 Hz. The first column is conventional beamforming. The middle column is FB with $\nu = 8$, and the right column incorporates $\epsilon = 0.2$ for RBF.

3 DISCUSSION

Robust Functional Beamforming provides the nearly the dynamic range of Functional Beamforming while removing the problem of peak loss due to steering vector errors. It depends on a parameter, ϵ which, at present, needs to be determined by trial and error.

REFERENCES

- [1] Merino-Martinez, R. G. Herold, M. Snellen, and R. P. Dougherty, "Assessment and comparison of the performance of functional projection beamforming for aeroacoustic measurements", BeBeC 2020-S7.
- [2] Merino-Martinez, R. M. Snellen and D.G. Simmons, "Functional Beamforming Applied to Full Scale Landing Aircraft", BeBeC-2016-D12.
- [3] Dougherty, R.P., "Functional Beamforming", Berlin Beamforming Conference, BeBeC 2014-1, 2014.
- [4] Dougherty, R.P., "Functional Beamforming for aeroacoustic source distributions", AIAA Paper 2014-3066, 2014.
- [5] Li J, Stoica P. Robust adaptive beamforming. John Wiley & Sons; 2005 Oct 10.

- [6] Bahr, C.J., W.M. Humphreys, D. Ernst, T. Ahlefeldt, C. Spehr, Q. Leclère, C. Picard, R. Porteous, D. Moreau, J.R. Fischer, and C. Doolan, "A Comparison of Microphone Phased Array Methods Applied to the Study of Airframe Noise in Wind Tunnel Testing," AIAA Paper 2017-3718.
- [7] Ahlefeldt, T., "Array Methods HDF5-Benchmark data" Downloaded from <https://www.b-tu.de/fg-akustik/cloud/> maintained by Thomas Geyer, January, 2020.
- [8] Dougherty, R.P., "Functional Beamforming Linear Programming for Determining Aeroacoustic Component Spectra", Submitted for the 28th AIAA/CEAS Aeroacoustics Conference, June, 2022.
- [9] Dougherty, R.P., "Enhancing Deconvolution with Functional Beamforming" BeBeC 2022-S1.